Effect of moderate DC electric field on formation of surfactant-laden drops

Alberini, Federico; Simmons, Mark; Kovalchuk, Nina

DOI:
10.1016/j.cherd.2020.03.009

Document Version
Publisher's PDF, also known as Version of record

Citation for published version (Harvard):
Alberini, F, Simmons, M & Kovalchuk, N 2020, 'Effect of moderate DC electric field on formation of surfactant-laden drops', *Chemical Engineering Research and Design*, vol. 157, pp. 133-141.
https://doi.org/10.1016/j.cherd.2020.03.009

Contents lists available at ScienceDirect

Chemical Engineering Research and Design

journal homepage: www.elsevier.com/locate/cherd

Effect of moderate DC electric field on formation of surfactant-laden drops

N. Kovalchuk, F. Alberini*, M.J.H. Simmons

School of Chemical Engineering, University of Birmingham, B152TT, UK

ARTICLE INFO

Article history:
Received 7 November 2019
Received in revised form 2 March 2020
Accepted 5 March 2020
Available online 14 March 2020

Keywords:
Emulsion
Electric field
Surfactant
Polarity

ABSTRACT

The continuous formation of mm-scale surfactant-laden aqueous drops in oil was studied under an applied DC electric field of 0–267 kV/m. The parameters varied included the flow rate of dispersed phase, the electric field strength, the viscosities and densities of dispersed and continuous phase and the surfactant type (anionic or cationic) and concentration. An increase in the electric field strength resulted in a decrease of the drop size due to increasing stresses on the drop interface. The size reduction continued until transition to the irregular regime. The values of critical electric field strength for this transition increased with an increase in both the flow rate and the viscosity ratio between the dispersed and continuous phase. The critical electric field strength and the size of the drops formed in the periodic dripping regime were independent of the electric field polarity. The effect of the electric field increased with a decrease of interfacial tension and density difference between the dispersed and continuous phase.

1. Introduction

The study of the behaviour of drops when subjected to an electric field began more than a century ago following the pioneering work of Rayleigh and then Zeleny and Taylor. Nowadays, the application of an electric field is used as a powerful control method for drop formation (Zhang and Basaran, 1996) and coalescence (Eow et al., 2001; Mhatre et al., 2015) in multiphase systems. In particular, electro-coalescence is used across a broad range of applications from drop microfluidics (Guzman et al., 2015) to oil and liquid–liquid extraction industry (Eow and Ghadiri, 2002; Suemar et al., 2012), whereas the electro-hydrodynamic method (Yogi et al., 2001) enables generation of micro-arrays of drops of orders of magnitude smaller than the nozzle size for ink jet printing, DNA sequencing, drug screening etc.

According to the seminal work of Taylor (1964), a conductive aqueous drop surrounded by air, or another immiscible non-conducting fluid, subjected to electric field of strength, E, elongates in the direction of the field. Beyond a critical value of E, the drop elongation becomes such that it loses its stability, this corresponds to the major to minor axis ratio based upon an elliptical drop of 1.9. Once the drop has lost its stability, a Taylor cone (cone angle of 98.6°) is formed at the end of the breaking drop emanating a thin jet or small drops. This effect was also observed for much less conductive oils (Taylor, 1969) and is now used in electrospinning (Teo and Ramakrishna, 2006; Bhardwaj and Kundu, 2010; Luo et al., 2012) and electrospraying (Jaworek, 2007; Rosell-Llompart et al., 2018; Gañán-Calvo et al., 2018) for broad range of applications including biomedical and pharmaceutical (Boda et al., 2018; Sill and von Recum, 2008; Shahriari et al., 2016; Sridhar et al., 2015; Miguel et al., 2018), food (Drosou et al., 2016; Anu Bhushani and Anandharamakrishnan, 2014), energy (Cavaliere et al., 2011; Peng et al., 2016) and membranes (Ahmed et al., 2015; Liao et al., 2018).

When compared to the huge number of publications on transport, deformations and instabilities of free drops due to an applied electrical field as well as the regime transitions of electro-hydrodynamic atomization (Cloupeau and Prunet-Foch, 1994; Shiryaeva and Grigor'ev, 1995; Jaworek and Krupa, 1999; Yazdekhasti et al., 2019) and electrospinning and electrospraying, much less attention has been paid to drop formation assisted by electric fields of moderate strength (far from formation of the Taylor cone) despite the fact that using an electric field can considerably improve emulsification processes. Note that the process of drop formation under the action of a moderate electrical field is different from free drop deformation under the same field because (i) the drop forming in contact with an electrode can acquire a contact charge proportional to E (Cho, 1964), which affects the electrical force applied to the drop and (ii) there is always an additional force involved in drop formation due to the mechanical moment of the dispersed

* Corresponding author.
E-mail address: f.alberini@bham.ac.uk (F. Alberini).
https://doi.org/10.1016/j.cherd.2020.03.009

phase, which should be taken into account together with a normal stress (Allan and Mason, 1962) from the electrical field, possible shear stress (Saville, 1997) and capillary pressure.

Studies of equilibrium shapes of pendant drops emerging from a capillary or from a hole in a metallic plate under moderate to strong electric field (Harris and Basaran, 1993; Joffre et al., 1982) have been followed by studies of kinetics of drop formation both experimentally (Zhang and Basaran, 1996; Huo et al., 2015; Lee et al., 2013) and numerically (Notz and Basaran, 1999; Ouedraogo et al., 2017; Borthakur et al., 2018).

It has been found that an increase in the strength of the applied electric field results in a considerable decrease of the size of the formed drops. This decrease is easily understood: if the electric field acts in the same direction as gravity, net forces acting to detach drop increase because of the additional electric field. At the same time the length of the thread connecting the detaching drop to the liquid cone remaining on the capillary increases, resulting in an increase of the size of satellite droplets (Zhang and Basaran, 1996; Lee et al., 2013). The formation of satellite drops is usually an undesirable event in emulsification processes as it reduces emulsion homogeneity, therefore their fate is important. According to (Zhang and Basaran, 1996), in the case of electrically assisted emulsification, small satellites always coalesced with the liquid cone, whereas according to (Huo et al., 2015), if E is high enough, the electric field hinders coalescence of the satellite drop with the liquid cone due to electrostatic repulsion of acquired surface contact charges. Therefore, further study of the satellite drops is necessary to precisely outline the conditions for their favorable coalescence either with the liquid cone or main drop. At certain strength of electric field the primary pinch-off point has been observed previously to move from the main drop to the liquid cone (Zhang and Basaran, 1996; Lee et al., 2013).

Normally, surfactants are used in emulsification processes to stabilize drops against coalescence. The presence of surfactants can affect considerably the kinetics of drop formation and the size of forming drops not only by reducing interfacial tension, but also due to dynamic effects of surfactant adsorption (Liao et al., 2004; de Saint Vincent et al., 2012; Kovalchuk et al., 2016, 2017). Moreover, the interaction of surfactant molecules, especially in the case of ionic surfactant with an electric field can have an additional effect. Surprisingly, the effect of surfactant has been studied only for deformation and break-up of (initially spherical) free drops due to DC electric field (Luo et al., 2018), however attention in this study was paid mostly to break up mode. This study fills this existing gap by examination of the formation of surfactant-laden drops under action of DC electric fields of moderate strength.

2. Material and methods

2.1. Experimental set-up

All experiments have been carried out in an experimental set-up constructed in our laboratory, shown in Fig. 1. A rectangular cell made of Perspex with dimensions L × W×H = 120 × 120 × 270 mm was filled with the continuous phase, either Lytol white mineral oil (Sonneborn) or an alternative mineral oil (Sigma, product number M8410).

Drops of the dispersed phase were formed periodically at the tip of a metallic capillary with an outer diameter of 2.1 mm by feeding the dispersed phase into the oil through a capillary at different flow rates. A TREK model 20/20C HS high voltage amplifier provided a potential of up to 8 kV. Two different configurations were used. In the first, the capillary served as an electrode connected to the amplifier. In the second, the capillary was placed inside a cylindrical metallic casing serving as an electrode. In this case, the capillary was insulated from the electrode by a glass tube with a wall thickness of 0.95 mm and there was no electrical contact between the dispersed phase and electrode.

Table 1 – Properties of aqueous solutions.

Solute	Concentration, mM	Electrical conductivity mS/m	Interfacial tension with Lytol, mN/m
	0	0.02	48
NaBr	7.5	0.97	48
	10	0.97	12
C_{12}Tab	20	1.591	8
	30	1.851	8
	10	0.611	8
SDS	20	0.889	8
	30	1.16	8
	10[a] + 4.88[b]	0.97	8
SDS + NaBr	20[a] + 7.2[b]	1.591	8
	30[a] + 6.8[b]	1.851	8

[a] Concentration of SDS.
[b] Concentration of NaBr.

The dispersed phase was fed to the capillary by a Harvard PHD 2000 Syringe Pump equipped with a 60 mL plastic syringe (BD Plastipak) through a pipe with a diameter of 4.8 mm. A grounded metallic ring, which served as a second electrode, was placed 30 mm below the capillary tip. Thus drop formation was studied under a DC electric field of a strength up to 267 kV/m. The effect of the reversal of electrode polarity was also systematically studied.

The syringe pump and the rectangular cell were situated inside a protective Perspex case, secured by a Guardmaster Safety Switch connected directly to the amplifier. The amplifier could only be activated when the switch was in the fully locked position. A time lag of 30 s built into the switch before unlocking ensured that the equipment was fully discharged before handling.

The flow rates were varied in the range 0.1–5 mL/min. Water as well as 30 and 60% v/v solutions of glycerol (Alfa Aesar, ultrapure, HPLC grade) in water were used as the dispersed phase which was either surfactant-laden or surfactant-free.

2.2. Physical properties of the continuous and the dispersed phases

Double-distilled water was produced using an Aquatron A 4000 D still (Stuart). Two surfactants were studied, either cationic, (dodecyltrimethylammonium bromide, C_{12}TAB, 99%, Acros Organics) or anionic (sodium dodecylsulphate, SDS, ≥99%, Sigma-Aldrich). The conductivity of dispersed phase was adjusted using sodium bromide, NaBr (≥99.5%, Sigma). Concentrations, corresponding conductivities and interfacial tensions of surfactant solutions in water are presented in Table 1 with the properties of oils and surfactant-free dispersed phases listed in Table 2. Surfactant-laden water/glycerol mixtures contained 30 mM of C_{12}TAB.

The addition of surfactant did not change the densities and viscosities of dispersed phases, but it changed the electrical conductivity, due to the ionic nature of the surfactants, and the interfacial tension (Table 1). Interfacial tension decreases with an increase of surfactant concentration up to critical micelle concentration (CMC); after which it remains nearly constant. CMC value for SDS is 8.2 mM and that for C_{12}TAB is 15 mM. Most of the studied solutions have concentrations above CMC and, for both surfactants, interfacial tension at concentrations above CMC is similar, 8–9 mN/m. A single used concentration

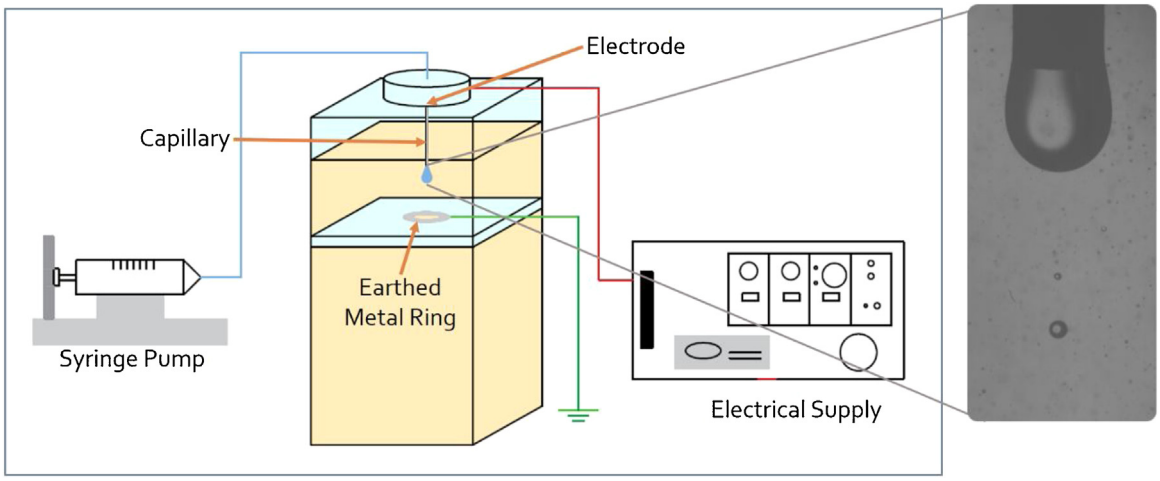

Fig. 1 – Sketch of experimental set-up.

Table 2 – Physical properties of dispersed (with 30 mM of C_{12}TAB[a]) and continuous phases.

Liquid	Density, kg/m^3	Viscosity, mPa·s	Relative permittivity (Anon, 1963; Bartnikas, 1994)	Electrical conductivity, mS/m
Water	998	1.0	80	1.9
30% glycerol/water	1075	2.6	72	1.1
60% glycerol/water	1158	11.0	62	0.4
Lytol	820	6.4	2	Non-conductive
Mineral oil[a]	840	32.8	2	Non-conductive

[a] Interfacial tension of 30 mM aqueous solution of C_{12}TAB vs mineral oil is ~9 mN/m.

of 10 mM of C_{12}TAB is below the CMC and has higher interfacial tension. The high surfactant concentrations were chosen in this study to make it consistent with formulations used in emulsification processes.

The electrical relaxation time $\tau_e = \varepsilon\varepsilon_0/K$, where ε is the relative electrical permittivity, ε_0 is the electrical permittivity of vacuum, $\varepsilon_0 = 8.85 \times 10^{-12}$ F/m, and K is the electric conductivity of dispersed phase, is below 1 μs for all studied surfactant solutions and around 35 μs for pure water. The characteristic time of drop formation $\tau_f = R^3/Q$, where R is the capillary radius and Q is the flow rate, is above 14 ms, i.e. $\tau_e \ll \tau_f$ and the dispersed phase can be considered as a perfect conductor. Note, the drop formation time observed in experiments was even larger than 100 ms for all considered cases, i.e. the inequality $\tau_e \ll \tau_f$ was confirmed experimentally.

The drop formation was recorded by a high speed camera (Photron FASTCAM SA3), equipped with a Navitar 12× ZoomXtender lens at 500–4000 fps. A KRUSS Optronic cold light source was used as a back light. The freeware software ImageJ (Schneider et al., 2012) was used for image processing.

The equilibrium interfacial tension was measured using a tensiometer K100 (Krüss) equipped with a platinum Wilhelmy plate. The viscosity was measured by a TA instruments Discovery-HR-2 rheometer in flow mode using cone and plate geometry with an angle of 2O 0′ 29″ and a truncation of 55 μm.

3. Results and discussion

3.1. *Transition from periodic dripping to irregular regimes*

Drop size in the absence of an electric field is determined by the interplay between gravity and interfacial tension with some contribution of the mechanical moment of the dispersed phase. The effect of gravity can be estimated from the gravitational Bond number

$$Bo = \frac{\Delta\rho g L^2}{\sigma} \quad (1)$$

where ρ is the density difference between dispersed and continuous phase, L is the characteristic length scale, chosen here as the capillary diameter, g is the acceleration due to gravity and σ is the interfacial tension between the dispersed and continuous phase. In the present study, see Tables 1 and 2, $0.85 < Bo < 1.83$ with larger values applicable for water/glycerol mixtures.

The flow rate used in this study varies between Q = 0.1 mL/min and Q = 5 mL/min, which corresponds to values of the Weber number,

$$We = \frac{\rho U^2 L}{\sigma} = \frac{16\rho Q^2}{\sigma\pi^2 L^3}, \quad (2)$$

$0.00006 < We < 0.16$. In Eq. (2) ρ is the density of the dispersed phase and U is the velocity of dispersed phase. Comparing the ranges of Bo and We number, it can be concluded that the effect of gravity is dominant and the effect of liquid flow is expected to be noticeable only for flow rates larger than 1 mL/min.

The addition of glycerol practically does not influence the interfacial tension of surfactant solutions at concentrations above CMC (Kovalchuk et al., 2016, 2018). This was confirmed also by our measurements giving interfacial tension of 30 mM solutions of SDS and C12TAB in 60% glycerol/40% water mixture with mineral oil around 9 mN/m, close to interfacial tension of solutions in water. Taking into account that the solutions of SDS and C_{12}TAB have similar interfacial tension at concentrations above the CMC, the size of formed drops in the

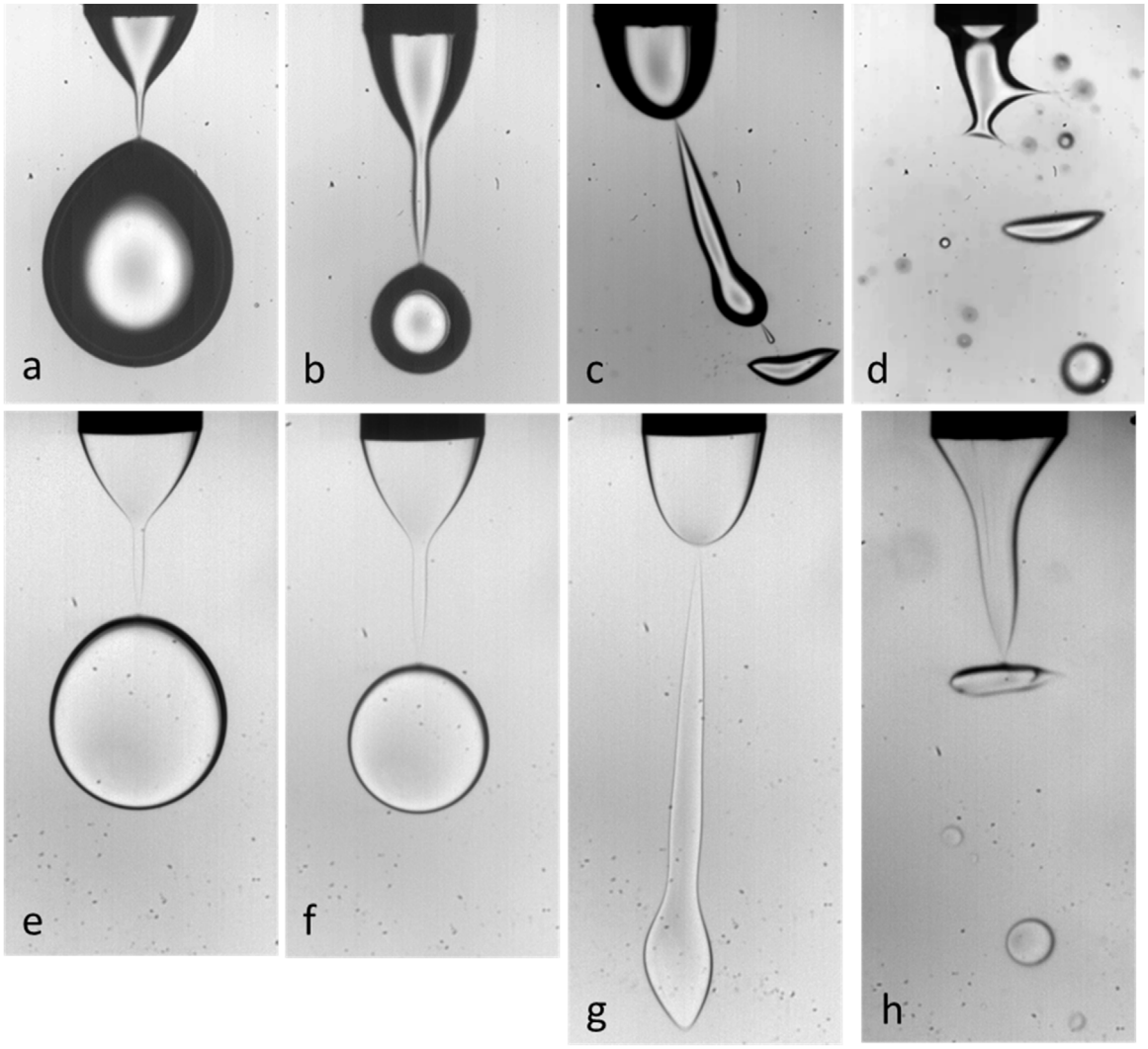

Fig. 2 – Changes in the drop size and formation regime with an increase of electric potential. Continuous phase – Lytol, flow rate of dispersed phase 1 mL/min. Dispersed phase – upper panel – solutions of 20 mM of SDS in water, bottom panel, solutions of 30 mM C_{12}TAB in 60% glycerol/40% water mixture: a – without electrical field, b – 2 kV, c – 4 kV, d – 30 mM + NaBr, 4 kV, e – without electric field, f – 2 kV, g – 4 kV, h – 7.4 kV.

absence of an electric field depends mainly on the density difference between the oil and aqueous phase. This is illustrated by Fig. 2a and e. The density difference between the Lytol and 60% glycerol/40% water mixture is nearly 2 times larger than the density difference between Lytol and water and therefore the size of water drop is larger.

The effect of the applied electric field can be characterised by the electrical capillary number (Luo et al., 2018; Castillo-Orozco et al., 2017; Pillai et al., 2016) sometimes also called electrical Weber number (Eow et al., 2003), or electrical Bond number (Huo et al., 2015), representing the relative importance of electric forces and interfacial tension:

$$Ca_{El} = \frac{\varepsilon\varepsilon_0 E^2 L}{\sigma} = \frac{\varepsilon\varepsilon_0 \varphi^2 L}{\sigma d^2} \quad (3)$$

where ε is the relative electric permittivity of continuous phase, ε_0 is the electric permittivity of vacuum, E is the strength of electrical field, ϕ is the electrical potential of the electrode and d is the distance between the electrode and the grounded ring. In the presented study Ca_{El} the only varied parameter in equation (Mhatre et al., 2015) was electrode potential ϕ; therefore ϕ represents unambiguously the electrical capillary number. Note, the relative permittivity presented in Table 2 is the minimum value characteristic for pure oils. The permittivity of oils used in this study can be a little bit higher due to impurities or dissolved water (Macioszek et al., 2019).

As can be seen in Fig. 2, an increase of the electrical field strength results in a decrease of the drop size and an elongation of the liquid filament connecting the detaching drop with the liquid cone at the capillary. Because of the larger contribution of gravity, the effect of electrical field on the size of a glycerol/water drop is weaker than its effect on the water drop (see the next section for the details), as can be seen in Fig. 2a, b, e, f. The elongation of the liquid filament means that the size of the satellite drops accompanying the formation of the main drop, increases (Fig. 2a and b, 2 e and f). The deviations from drop mono-dispersity increase and simultaneously the size of satellite drops approach the size of the main drop. Eventually transition to an irregular regime occurs, such as electro-hydrodynamic jetting (Zhang and Basaran, 1996; Lee et al., 2013), spindle (Rosell-Llompart et al., 2018; Huo et al., 2015) or micro-dripping (Castillo-Orozco et al., 2017) (Fig. 2c, d, g, h) before formation of the Faraday cone. Note that the aim of this work is only to delineate the transition from the regular drop formation to an irregular regime. More information on

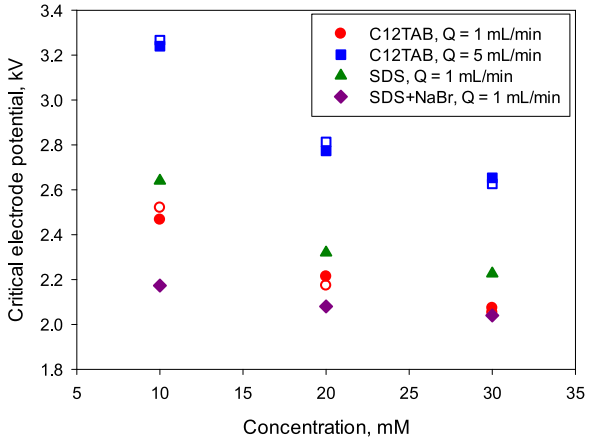

Fig. 3 – Dependence of critical electrode potential at transition to irregular regime on surfactant concentration. Filled symbols correspond to positive potential, empty symbols correspond to negative potential of electrode.

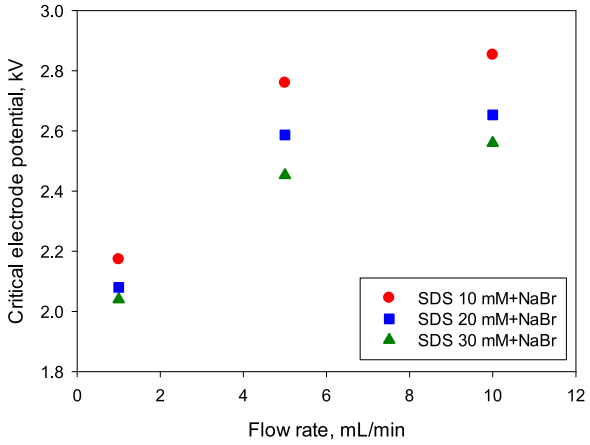

Fig. 4 – Dependence of critical electrode potential at transition to irregular regime on the flow rate of dispersed phase for solutions of SDS + NaBr is water.

different regimes appearing after the transition can be found for example in (Rosell-Llompart et al., 2018).

It must be noted that different criteria are used to mark the transition to irregular regime in the literature (Zhang and Basaran, 1996; Huo et al., 2015; Lee et al., 2013). Here we consider the regime being irregular if it becomes impossible to distinguish between the main drops and the satellites. The different topologies of drop formation in the irregular regime can be achieved by changing the applied voltage, and also by changing the conductivity of the dispersed phase (Fig. 2c, d: the same applied voltage). The dependence of the topology of drop formation on the conductivity of dispersed phase was reported also in (Lee et al., 2013). The viscosity of the dispersed phase also influences topology after transition (Fig. 2c, g).

The dependence of the critical electrode potential at the transition to the irregular regime on various parameters is quantified in Fig. 3 for solutions prepared in water. In particular, it shows that an increase in the concentration of surfactant results in a decrease of critical electrode potential. Considering that for both SDS and SDS + NaBr, all studied concentrations are above CMC and therefore interfacial tension remains nearly constant, the only parameter that changes with an increase of concentration is electrical conductivity. Therefore, it can be concluded that this decrease in critical electrode potential is due to an increase in electrical conductivity of dispersed phase. This conclusion is in line with potential difference between SDS and SDS + NaBr as well as between SDS and C_{12}TAB solution at flow rate 1 mL/min. However solutions of C_{12}TAB and SDS + NaBr have the same conductivities at the same molar concentrations, whereas the critical electrode potential for SDS + NaBr is lower. This example shows that the nature and location of charges (free charges of micelle-bound) can also affect the value of the critical transition potential.

Comparison made between the data for C_{12}TAB at flow rates of 1 and 5 mL/min shows that an increase in the flow rate makes system more resistant to instability. This is possibly explained by the effect of the pressure force generated by the flow of the dispersed phase which increases with flow rate. This results in an increase in size of the tail of the cone. Hence, more mass per unit time enters into the drop volume (as expected from a simple mass balance) which requires more electric potential to achieve the same effect which was achieved at lower flow rate. Thus, to reach the same critical point more energy per unit mass is needed hence a higher electrode potential.

As it can be observed from Fig. 3, at fixed flow rate, the difference between surfactants and surfactant plus NaBr decreases with an increase of concentration above CMC (CMC = 8.2 mM for SDS and 15 mM for C_{12}TAB). The presence of NaBr lowers the CMC for the SDS solution. This results in rather similar critical electrode potential values being observed at all studied concentrations for this composition. Moreover, at 30 mM, C_{12}TAB solution and SDS + NaBr solution have the same electrical conductivity and achieve a similar value of the critical potential. Noticeably, the polarity of the electric field (positive or negative) has practically no effect on the critical electrode potential as most of the points overlap.

This is confirmed also by the data presented in Fig. 4, where the dependence of the critical electrode potential on flow rate is shown for three different concentrations of SDS + NaBr solutions. The critical potential increases, with an increase of flow rates, whereas an increase in the electrical conductivity results in a decrease of the critical potential at a given flow rate. Similar results have been observed also for solutions of C_{12}TAB in glycerol/water mixtures (30% and 60% of glycerol) and for two different continuous phases (Lytol and mineral oil). The critical potential increases with an increase of glycerol concentration and this increase is more pronounced in the mineral oil compared to Lytol. The critical potential for the same dispersed phase is lower in mineral oil than in Lytol. Therefore, it can be assumed that the critical potential changes in line with the viscosity ratio of dispersed and continuous phase. However, more thorough study is necessary to validate this hypothesis.

3.2. *Effect of electric field on drop size at periodic dripping*

Similar drop sizes have been obtained in comparative experiments with the electrically insulated capillary and the capillary serving as an electrode. Therefore, under conditions of the present study the effect of the contact charge can be neglected.

Fig. 5 shows the dependence of drop size on surfactant concentration with and without electric field for solutions in water at flow rate of dispersed phase of 1 mL/min. The concentration is normalised by the corresponding values of CMC: 8.2 mM for SDS and 15 mM for C_{12}TAB. Addition of salt results in

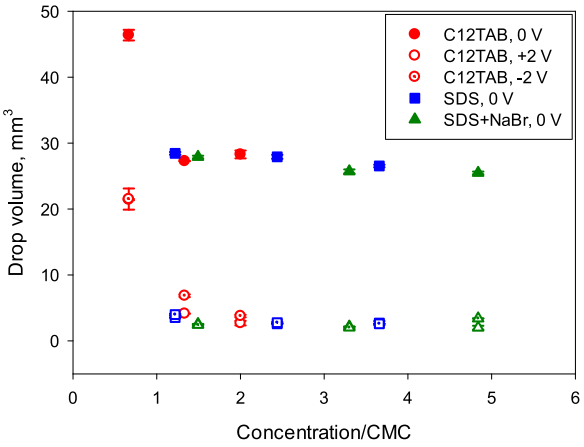

Fig. 5 – Dependence of size of surfactant-laden drops of water on normalised concentration of C_{12}TAB, SDS and SDS + NaBr with and without electric field for flow rate 1 mL/min. Filled symbols correspond to the case without electric field, empty symbols correspond to positive potential at capillary and dotted symbols correspond to negative potential at capillary. Interfacial tension is similar for all compositions above CMC.

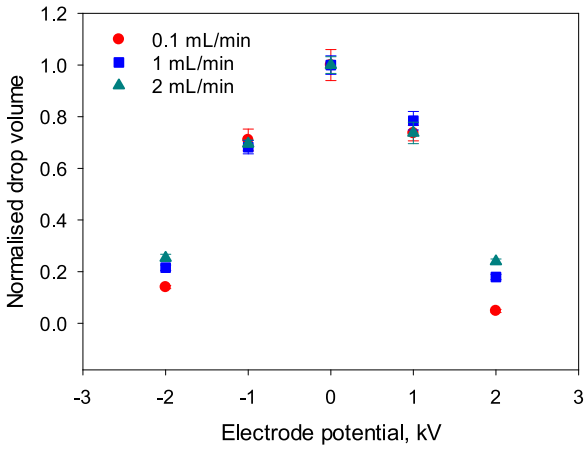

Fig. 6 – Effect of flow rate and electric field potential and polarity on drop size: continuous phase – Lytol, dispersed phase – C_{12}TAB in 30% glycerol/water mixture. Drop volume was normalised by the volume in the absence of electric field.

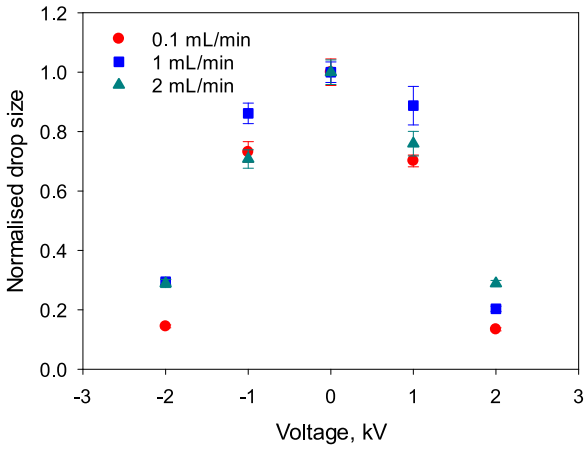

Fig. 7 – Effect of flow rate and electric field potential and polarity on drop size: continuous phase – mineral oil, dispersed phase – C_{12}TAB in 30% glycerol/water mixture. Drop volume was normalised by the volume in the absence of electric field.

a decrease of CMC value, therefore for composition SDS + NaBr the CMC values, c_{CMC} have been calculated using the equation reported previously (Kovalchuk et al., 2016; Anon, 2001):

$$c^*_{CMC} = f((c_{CMC} + c_{NaBr})\, c_{CMC})^{0.5} \quad (4)$$

where c^* is the CMC without salt, c_{NaBr} is the concentration of $NaBr$ and f is the average activity coefficient of the ions in the bulk. For 1:1 electrolyte, NaBr, $log\,(f) = -\frac{0.5115\sqrt{I}}{1+1.316\sqrt{I}} + 0.055I$, where $I = c_{NaBr}$ is the ionic strength of the solution.

The choice of those three different systems (water with surfactant solutions of C_{12}TAB, SDS and SDS + NaBr) was driven by the desire to understand the effect of surfactant polarity versus electric field polarity and effect of electrical conductivity of the solutions. In particular, as surfactants should redistribute under the action of an electric field, this can result in different surfactant concentrations and therefore different interfacial tension in the neck region, affecting drop size. The range of concentrations from ~0.5 CMC up to ~5 CMC has been investigated. It is clear from Fig. 5 that the electric field reduces considerably the size of forming drop and this reduction is independent, at least at concentrations above the CMC, of surfactant nature (cationic or anionic) and polarity of applied electric field. Therefore, it can be concluded that the changes in surface tension due to surfactant redistribution under the electric field are very small compared with electrical forces acting on the drop. Probably this is the result of using high surfactant concentrations, when the dependence of surface tension on surfactant concentration is relatively small and dependence of the drop size on polarity can be observed at smaller concentrations.

The drop size is independent of the electrical conductivity of the solution (C_{12}TAB and SDS + NaBr water solutions have higher electrical conductivity than aqueous solutions of SDS) in contrast to what was observed for the critical electrode potential. This means that during drop formation in the regular dripping regime, the dispersed phase behaves as a perfect conductor.

To further validate the above discussion, experiments have been run at different flow rates and different electrode potentials using a 30 mM solution of C_{12}TAB in water/glycerol mixtures. As shown in Fig. 6, an increase of the electrode potential at fixed flow rate results in a monotonic decrease of the drop size, again with no systematic difference between the two polarities. According to Fig. 6, where the drop size was normalised by the drop size at the same flow rate in absence of electric field, the relative decrease looks similar at an electrode potential of 1 kV, but at 2 kV the size decreases faster at smaller flow rates, for both polarities of the electric field. Replacing Lytol with mineral oil, i.e. a 5-fold increase of the viscosity ratio between the continuous and dispersed phase and a 10% decrease in buoyancy force, it is noticeable that the dependence of the normalised drop volume on electrode potential (Fig. 7) does not change. Note, the results in Figs. 6 and 7 are normalised by the drop size in the absence of the electric field. This value is dependent on the density difference between the dispersed and the continuous phase, i.e. the normalising drop size is larger in Fig. 6.

As shown in Fig. 8, the effect of electric field on drop size in much stronger at lower interfacial tension (compare water with and without surfactant). When a water/glycerol mixture is used instead of water, there is a weak effect up to an elec-

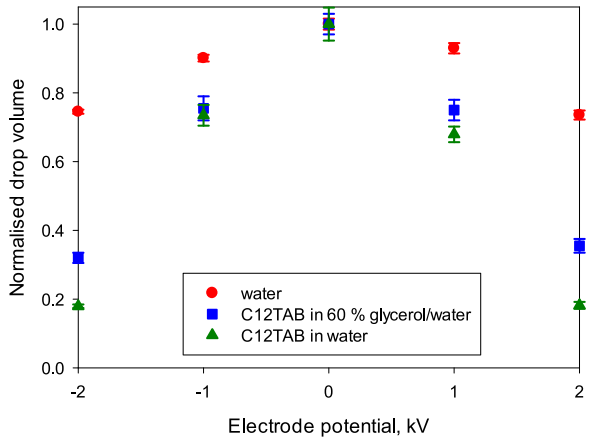

Fig. 8 – Effect of composition of dispersed phase and electric field polarity on drop size: continuous phase – mineral oil, dispersed phase – water, C_{12}TAB in 60% glycerol/water mixture and C_{12}TAB in water. Flow rate – 1 mL/min. Drop volume was normalised by the volume in the absence of electric field.

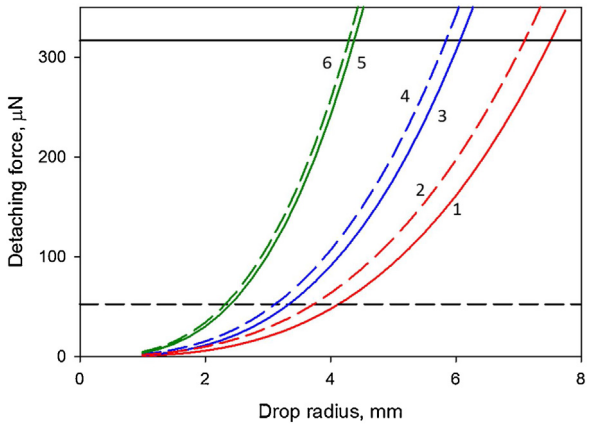

Fig. 9 – Dependence of force detaching drop from the capillary on drop radius (left hand side of Eq. (5)). Continuous phase – Lytol: 1 – water drop without electrical field, 2 – water drop in electrical field of 2 kV, 3 – 60% glycerol/40% water drop without electrical field, 4 – 60% glycerol/40% water drop in electrical field of 2 kV. Hypothetical case representing the density difference between dispersed and continuous phase of 900 kg/m: 5 – without electrical field, 6 – electrical field of 2 kV. Solid horizontal line shows the interfacial tension force for the drop without surfactant, interfacial tension 48 mN/m, dashed horizontal line correspond to the interfacial tension force at 8 mN/m.

trode potential of 1 kV; above 2 kV the water/glycerol mixture causes a slower relative decrease in drop size. This might be due to the combination of viscous forces, relative permittivity and electrical conductivity, but the main contribution gives the change in density difference.

The results presented in Fig. 8 can be understood by using the force balance at drop detachment. Detachment occurs when the sum of gravity and electrical forces exceeds the interfacial tension force, i.e.

$$\frac{4}{3}\pi R^3 \Delta\rho + 4\pi R^2 \varepsilon\varepsilon_0 \frac{\varphi^2}{d^2} > \pi L\sigma \qquad (5)$$

where R is the drop radius. Note, expressions for electrical and gravity forces in Eq. (5) are only approximations assuming a spherical drop shape and interfacial tension can differ from the equilibrium value, therefore this equation can be only used for a qualitative analysis. The dependence of the detaching force on drop radius for several cases of interest is presented in Fig. 9, where the characteristic values of the surface tension force given by the right hand side of Eq. (5) are shown by horizontal lines. To display the trends more clearly, the hypothetical case of a very large density difference between the continuous and dispersed phase, which can be observed for drop formation in air, is added to Fig. 9.

Obviously, the size of the drop decreases with an increase of density difference or decrease of interfacial tension both in the presence and in the absence of electric field. Results presented in Fig. 9 show, however, that for the strengths of electric field enabling drop formation in the periodic dripping regime the effect of the electric field is smaller than that of the density difference, especially at large interfacial tension. The change in the interfacial tension from 48 to 8 mN/m in the absence of electric field results in a decrease of the water drop radius from 7.5 to 4.1 mm ($R \sim \sigma^{1/3}$). At the same time, the decrease in the drop size due to an applied potential of 2 kV remained practically the same at 0.4 mm for both, surfactant-laden and surfactant-free drop. Thus, the relative drop size in the presence of electric field decreases much faster at low interfacial tension.

It is clear from Eq. (5) and Fig. 9 that an increase in the density difference decreases the contribution of electric field in the detaching force. The size of the drops formed in the absence of the electric field decreases as well, but for example by replacement of water by 60% glycerol/40% water mixture, the drop size decreases by a factor of 1.2, from 4.4 to 3.3 mm, whereas the decrease in the drop size due to electrical field decreased from 0.4 to 0.22 mm, i.e. by a factor of 1.8. Therefore the relative deformation in the same electric field is smaller for glycerol/water drop compared to the water drop of the same interfacial tension as shown in Fig. 8.

4. Conclusions

Formation of conductive surfactant-laden drops of mm-size in an oil continuous phase was studied under conditions of an applied DC electric field of moderate strength. The periodic dripping regime under conditions We < 0.16 and 0.85 < Bo < 1.83 was observed at $Ca_{El} < 1.7 \times 10^{-4}$. The critical electrical capillary number delimiting the transition to irregular regimes increases with an increase of both the flow rate of continuous phase and the viscosity ratio between the dispersed and continuous phases. Despite a very small electrical relaxation time when compared with the formation time of drops, the critical electrical capillary number depends on the electrical conductivity of dispersed phase. The nature of this dependency is unclear and requires further investigation. The critical electrical capillary number is independent of the electric field polarity for both cationic and anionic surfactants at concentrations close or above CMC.

The size of drops formed in the periodic dripping regime is independent of the polarity of electric field and the presence or absence of direct contact of the forming drop with the electrode. Application of the electric field enabled reduction of the drop volume by up to 10 times whilst remaining in the periodic regime. The effect of electric field is more pronounced at small

interfacial tension and small density differences between the dispersed and continuous phases.

Conflict of interests

The authors declare that they have no conflict of interest.

Acknowledgments

Support from the Engineering & Physical Sciences Research Council, UK, through the PREMIERE programme grant EP/T000414/1is gratefully acknowledged. Ms E. Jenkins, Mr. B. Harwood, Mr C.M. Sunderland, Mr G. Giambalvo and Mr M. Aghamirzayev are acknowledged to have contributed some of the results of their Masters theses to this work.

References

Ahmed, F.E., Lalia, B.S., Hashaikeh, R., 2015. A review on electrospinning for membrane fabrication: challenges and applications. Desalination 356, 15–30.

Allan, R.S., Mason, S.G., 1962. Particle behaviour in shear and electric fields I. Deformation and burst of fluid drops. Proc. R. Soc. Lond. A 267, 45–61.

Anon, 1963. Physical Properties of Glycerine and its Solutions. Glycerine Producers' Association, New York.

Anon, 2001. Surfactants: Chemistry, Interfacial Properties, Applications. Elsevier, Amsterdam, The Netherlands.

Zhang, X., Basaran, O.A., 1996. Dynamics of drop formation from a capillary in the presence of an electric film. J. Fluid Mech. 326, 239–263.

Notz, P.K., Basaran, O.A., 1999. Dynamics of drop formation in an electric field. J. Colloid Interface Sci. 213, 218–237.

Liao, Y.C., Subramani, H.J., Franses, E.I., Basaran, O.A., 2004. Effects of soluble surfactants on the deformation and breakup of stretching liquid bridges. Langmuir 20, 9926–9930.

Anu Bhushani, J., Anandharamakrishnan, C., 2014. Electrospinning and electrospraying techniques: potential food based applications. Trends Food Sci. Technol. 38 (1), 21–33.

Bartnikas, R., 1994. Permittivity and loss of insulating liquids. In: Bartnikas, R. (Ed.), Engineering Dielectrics. 3. Electrical Insulating Liquids. ASTM International, West Conshohocken, pp. 3–146.

Bhardwaj, N., Kundu, S.C., 2010. Electrospinning: a fascinating fiber fabrication technique. Biotechnol. Adv. 28 (3), 325–347.

Boda, S.K., Li, X., Xie, J., 2018. Electrospraying an enabling technology for pharmaceutical and biomedical applications: a review. J. Aerosol Sci. 125, 164–181.

Borthakur, M.P., Biswas, G., Bandyopadhyay, D., 2018. Dynamics of drop formation from submerged orifices under the influence of electric field. Phys. Fluids 30 (12).

Castillo-Orozco, E., Kar, A., Kumar, R., 2017. Electrospray mode transition of microdroplets with semiconductor nanoparticle suspension. Sci. Rep. 7 (1), 5144.

Cavaliere, S., Subianto, S., Savych, I., Jones, D.J., Rozière, J., 2011. Electrospinning: designed architectures for energy conversion and storage devices. Energy Environ. Sci. 4 (12).

Cho, A.Y.H., 1964. Contact charging of micron-sized particles in intense electric fields. J. Appl. Phys. 35 (9), 2561–2564.

Cloupeau, M., Prunet-Foch, B., 1994. Electrohydrodynamic spraying functioning modes: a critical riview. J. Aerosol Sci. 25, 1021–1036.

de Saint Vincent, M.R., Petit, J., Aytouna, M., Delville, J.P., Bonn, D., Kellay, H., 2012. Dynamic interfacial tension effects in the rupture of liquid necks. J. Fluid Mech. 692, 499–510.

Drosou, C.G., Krokida, M.K., Biliaderis, C.G., 2016. Encapsulation of bioactive compounds through electrospinning/electrospraying and spray drying: a comparative assessment of food-related applications. Dry. Technol. 35 (2), 139–162.

Eow, J.S., Ghadiri, M., 2002. Electrostatic enhancement of coalescence of water droplets in oil:a review of the technology. Chem. Eng. J. 85, 357–368.

Eow, J.S., Ghadiri, M., Sharif, A.O., Williams, T.J., 2001. Electrostatic enhancement of coalescence of water droplets in oil: a review of the current understanding. Chem. Eng. J. 84, 173–192.

Eow, J.S., Ghadiri, M., Sharif, A., 2003. Experimental studies of deformation and break-up of aqueous drops in high electric fields. Colloids Surf. A: Physicochem. Eng. Asp. 225 (1–3), 193–210.

Gañán-Calvo, A.M., López-Herrera, J.M., Herrada, M.A., Ramos, A., Montanero, J.M., 2018. Review on the physics of electrospray: from electrokinetics to the operating conditions of single and coaxial Taylor cone-jets, and AC electrospray. J. Aerosol Sci. 125, 32–56.

Guzman, A.R., Kim, H.S., de Figueiredo, P., Han, A., 2015. A three-dimensional electrode for highly efficient electrocoalescence-based droplet merging. Biomed. Microdevices 17 (2), 35.

Harris, M.T., Basaran, O.A., 1993. Capillary electrohydrostatics of conducting drops hanging from a nozzle in an electric field. J. Colloid Interface Sci. 161, 389–413.

Huo, Y., Wang, J., Zuo, Z., Fan, Y., 2015. Visualization of the evolution of charged droplet formation and jet transition in electrostatic atomization. Phys. Fluids 27 (11).

Jaworek, A., 2007. Micro- and nanoparticle production by electrospraying. Powder Technol. 176 (1), 18–35.

Jaworek, A., Krupa, A., 1999. Classification of the modes of EHD spraying. J. Aerosol Sci. 30, 873–893.

Joffre, G., Prunet-Foch, B., Berthomme, S., Cloupeau, M., 1982. Deformation of liquid menisci under the action of an electric field. J. Electrostat. 13, 151–165.

Kovalchuk, N.M., Nowak, E., Simmons, M.J., 2016. Effect of soluble surfactants on the kinetics of thinning of liquid bridges during drops formation and on size of satellite droplets. Langmuir 32 (20), 5069–5077.

Kovalchuk, N.M., Nowak, E., Simmons, M.J.H., 2017. Kinetics of liquid bridges and formation of satellite droplets: difference between micellar and bi-layer forming solutions. Colloids Surf. A: Physicochem. Eng. Asp. 521, 193–203.

Kovalchuk, N.M., Jenkinson, H., Miller, R., Simmons, M.J.H., 2018. Effect of soluble surfactants on pinch-off of moderately viscous drops and satellite size. J. Colloid Interface Sci. 516, 182–191.

Lee, M.W., Kim, N.Y., Yoon, S.S., 2013. On pinchoff behavior of electrified droplets. J. Aerosol Sci. 57, 114–124.

Liao, Y., Loh, C.-H., Tian, M., Wang, R., Fane, A.G., 2018. Progress in electrospun polymeric nanofibrous membranes for water treatment: fabrication, modification and applications. Prog. Polym. Sci. 77, 69–94.

Luo, C.J., Stoyanov, S.D., Stride, E., Pelan, E., Edirisinghe, M., 2012. Electrospinning versus fibre production methods: from specifics to technological convergence. Chem. Soc. Rev. 41 (13), 4708–4735.

Luo, X., Huang, X., Yan, H., Yang, D., Wang, J., He, L., 2018. Breakup modes and criterion of droplet with surfactant under direct current electric field. Chem. Eng. Res. Des. 132, 822–830.

Macioszek, Ł, Włodarczak, S., Rybski, R., 2019. Mineral oil moisture measurement with the use of impedance spectroscopy. IET Sci. Meas. Technol. 13 (8), 1158–1162.

Mhatre, S., Vivacqua, V., Ghadiri, M., Abdullah, A.M., Al-Marri, M.J., Hassanpour, A., et al., 2015. Electrostatic phase separation: a review. Chem. Eng. Res. Des. 96, 177–195.

Miguel, S.P., Figueira, D.R., Simoes, D., Ribeiro, M.P., Coutinho, P., Ferreira, P., et al., 2018. Electrospun polymeric nanofibres as wound dressings: a review. Colloids Surf. B: Biointerfaces 169, 60–71.

Ouedraogo, Y., Gjonaj, E., Weiland, T., Gersem, H.D., Steinhausen, C., Lamanna, G., et al., 2017. Electrohydrodynamic simulation of electrically controlled droplet generation. Int. J. Heat Fluid Flow 64, 120–128.

Peng, S., Li, L., Kong Yoong Lee, J., Tian, L., Srinivasan, M., Adams, S., et al., 2016. Electrospun carbon nanofibers and their hybrid composites as advanced materials for energy conversion and storage. Nano Energy 22, 361–395.
Pillai, R., Berry, J.D., Harvie, D.J., Davidson, M.R., 2016. Electrokinetics of isolated electrified drops. Soft Matter 12 (14), 3310–3325.
Rosell-Llompart, J., Grifoll, J., Loscertales, I.G., 2018. Electrosprays in the cone-jet mode: from Taylor cone formation to spray development. J. Aerosol Sci. 125, 2–31.
Saville, D.A., 1997. Electrohydrodynamics: the Taylor-Melcher leaky dielectric model. Annu. Rev. Fluid Mech. 29, 27–64.
Schneider, C.A., Rasband, W.S., Eliceiri, K.W., 2012. NIH image to ImageJ: 25 years of image analysis. Nat. Methods 9 (7), 671–675.
Shahriari, A., Kim, M.M., Zamani, S., Phillip, N., Nasouri, B., Hidrovo, C.H., 2016. Flow regime mapping of high inertial gas–liquid droplet microflows in flow-focusing geometries. Microfluid. Nanofluidics 20 (1).
Shiryaeva, S.O., Grigor'ev, A.I., 1995. The semiphenomenological classification of the modes of electrostatic dispersion of liquids. J. Electrostat. 34, 51–59.
Sill, T.J., von Recum, H.A., 2008. Electrospinning: applications in drug delivery and tissue engineering. Biomaterials 29 (13), 1989–2006.
Sridhar, R., Lakshminarayanan, R., Madhaiyan, K., Amutha Barathi, V., Lim, K.H., Ramakrishna, S., 2015. Electrosprayed nanoparticles and electrospun nanofibers based on natural materials: applications in tissue regeneration, drug delivery and pharmaceuticals. Chem. Soc. Rev. 44 (3), 790–814.
Suemar, P., Fonseca, E.F., Coutinho, R.C., Machado, F., Fontes, R., Ferreira, L.C., et al., 2012. Quantitative evaluation of the efficiency of water-in-crude-oil emulsion dehydration by electrocoalescence in pilot-plant and full-scale units. Ind. Eng. Chem. Res. 51 (41), 13423–13437.
Taylor, G., 1964. Disintegration of water drops in an electric field. Proc. R. Soc. Lond. A 280, 383–397.
Taylor, G., 1969. Electrically driven jets. Proc. R. Soc. Lond. A 313, 453–475.
Teo, W.E., Ramakrishna, S., 2006. A review on electrospinning design and nanofibre assemblies. Nanotechnology 17 (14), R89–R106.
Yazdekhasti, A., Pishevar, A., Valipouri, A., 2019. Investigating the effect of electrical conductivity on electrospray modes. Exp. Therm. Fluid Sci. 100, 328–336.
Yogi, O., Kawakami, T., Yamauchi, M., Ye, J.Y., Ishikawa, M., 2001. On-demand droplet spotter for preparing pico- to femtoliter droplets on surfaces. Anal. Chem. 73 (1896–1902).